CONF-960994--7

IBMM-96 Conference Proceedings - Nuclear Instruments and Methods in Physics Research, Section B

ENCAPSULATED NANOCRYSTALS AND QUANTUM DOTS FORMED BY ION BEAM SYNTHESIS

C. W. White, J. D. Budai, S. P. Withrow, J. G. Zhu, S. J. Pennycook, and R. A. Zuhr
Oak Ridge National Laboratory, Oak Ridge, Tenn.

D. M. Hembree Jr.
The Oak Ridge Y-12 Plant, Oak Ridge, Tenn.

D. O. Henderson
Fisk University, Nashville, Tenn.

R. H. Magruder
Vanderbilt University, Nashville, Tenn.

M. J. Yacaman and G. Mondragon
UNAM, Mexico

S. Prawer
University of Melbourne, Melbourne, Australia

"The submitted manuscript has been authored by a contractor of the U.S. Government under contract No. DE-AC05-96OR22464. Accordingly, the U.S. Government retains a nonexclusive, royalty-free license to publish or reproduce the published form of this contribution, or allow others to do so, for U.S. Government purposes."

Prepared by the
Oak Ridge National Laboratory
Oak Ridge, Tennessee 37831
managed by
LOCKHEED MARTIN ENERGY RESEARCH CORP.
for the
U.S. DEPARTMENT OF ENERGY
under contract DE-AC05-96OR22464

September 1996

DISTRIBUTION OF THIS DOCUMENT IS UNLIMITED

MASTER

DISCLAIMER

Portions of this document may be illegible in electronic image products. Images are produced from the best available original document.

Reference No. 401

ENCAPSULATED NANOCRYSTALS AND QUANTUM DOTS FORMED BY ION BEAM SYNTHESIS

C. W. White, J. D. Budai, S. P. Withrow, J. G. Zhu, S. J. Pennycook, and R. A. Zuhr
Oak Ridge National Laboratory, Oak Ridge, Tenn.

D. M. Hembree Jr.
The Oak Ridge Y-12 Plant, Oak Ridge, Tenn.

D. O. Henderson
Fisk University, Nashville, Tenn.

R. H. Magruder
Vanderbilt University, Nashville, Tenn.

M. J. Yacaman and G. Mondragon
UNAM, Mexico

S. Prawer
University of Melbourne, Parkville, Victoria, Australia

Abstract

High-dose ion implantation has been used to synthesize a wide range of nanocrystals and quantum dots and to encapsulate them in host materials such as SiO_2, α–Al_2O_3, and crystalline Si. When Si nanocrystals are encapsulated in SiO_2, they exhibit dose dependent absorption and photoluminescence which provides insight into the luminescence mechanism. Compound semiconductor nanocrystals (both Group III-V and Group II-VI) can be formed in these matrices by sequential implantation of the individual constituents, and we discuss their synthesis and some of their physical and optical properties.

Contact: C. W. White
Oak Ridge National Laboratory
P. O. Box 2008
Oak Ridge, TN 37931-6057

telephone: 423-574-6295
fax: 423-576-8135
e-mail: whitecw@ornl.gov

"The submitted manuscript has been authored by a contractor of the U.S. Government under contract No. DE-AC05-96OR22464. Accordingly, the U.S. Government retains a nonexclusive, royalty-free license to publish or reproduce the published form of this contribution, or allow others to do so, for U.S. Government purposes."

1. Introduction

Nanocrystals and quantum dots have attracted considerable interest recently because of their unusual properties, which result when structures are made sufficiently small that electrons can be confined to regions smaller than their delocalized length [1]. Many methods are currently being investigated to synthesize these structures and high-dose ion implantation is a technique which can be used to form a wide range of them. In this method, implantation creates a supersaturated impurity concentration in the near surface of a host matrix. Subsequent annealing leads to precipitation and the formation of nanocrystals which are encapsulated in the host material. The depth and depth distribution can be controlled to a certain extent by the implantation and annealing parameters.

Metallic nanocrystals such as Au [2,4] and Cu [5] have been formed in fused silica by implantation, and these lead to dramatic changes in the optical properties and give rise to a refractive index which depends on optical intensity, thus making these interesting candidates for nonlinear optical materials. This method has been used also to synthesize elemental semiconductor nanocrystals (Si, Ge) in fused silica [6-15]. These emit strong photoluminescence (PL) in the visible and near IR, but the mechanism responsible for this radiation is currently under investigation. Si and Ge nanocrystals have been produced in α-Al_2O_3 by ion implantation [16], and these are three dimensionally oriented with respect to the lattice. Finally, sequential implantation of various combinations of ions can be used to produce compound semiconductor or alloy nanocrystals in several host materials [12, 17-25]. Implantation may provide an attractive method for producing some of these compound nanocrystals because of their sensitivity to high temperatures or oxidizing conditions.

In this paper, we present results on the synthesis, characteristics, and properties of nanocrystalline composites formed by ion implantation. We will discuss the formation and optical properties of silicon nanocrystals in fused silica. We will show also that compound semiconductor nanocrystals (Group III-V and Group II-VI) can be formed by sequential

implantation into matrices SiO_2, α-Al_2O_3, and crystalline Si. Nanocrystals are randomly oriented in an amorphous matrix, but are three dimensionally oriented in a crystalline matrix. The order of implantation is very important in determining the size of the compound nanoparticles. We also show the efficiency for forming compounds by this sequential implantation process is large.

2. Experimental procedures

Substrates used in this work were fused silica (Corning 7940), thermally oxidized silicon wafers (SiO_2/Si), c-axis oriented α-Al_2O_3, or Si(100) wafers. Ions were implanted into these matrices to doses of order $10^{17}/cm^2$ and at energies chosen to give a projected range of 100 nm or more. To form compounds or alloys, various combinations of ions were implanted at energies chosen to give overlap of the profiles. All samples were annealed in flowing Ar + 4% H_2 to induce precipitation and nanocrystal formation. Characterization was carried out using a variety of techniques including x-ray diffraction (Cu-Kα, radiation), cross-sectional transmission electron microscopy (TEM), Rutherford backscattering (RBS) and ion channeling measurements, and various optical property measurements (absorption and PL).

3. Silicon nanocrystals in SiO_2

Silicon and germanium nanocrystals can be synthesized in SiO_2 by ion implantation followed by annealing [6-15] and such samples give rise to strong PL in the visible and near IR regions. Figure 1 is a cross-section TEM micrograph showing Si nanocrystals formed in SiO_2 films (~8500 Å thick) on silicon. Multiple energy implants were used to produce excess Si concentrations of $5 \times 10^{21}/cm^3$ or $2 \times 10^{22}/cm^3$ throughout the films. Implanted samples were annealed to cause precipitation and nanocrystal formation. The micrograph shows that the average size of the nanocrystals in the lower concentration sample is ~25 Å diameter, while at the higher concentration the average size is larger (up to ~45 Å diameter) but not as uniform in size.

Figure 2 shows PL spectra (excited at 488 nm) from fused silica implanted by Si (400 keV, $6 \times 10^{17}/cm^2$, RT). The peak concentration of excess Si is ~$2 \times 10^{22}/cm^3$. In the as-implanted state, luminescence centered at ~6500 Å is observed which is believed [7] to arise from defects introduced into the SiO_2 matrix during the implantation process. Annealing in Ar + 4% H_2 at 1100°C gives rise to the formation of Si nanocrystals, and strong PL peaked at 7500 Å is observed. The intensity of the luminescence at ~7500 Å is strongly affected by hydrogen, as others have noted [13]. Annealing in pure Ar or in vacuum will reduce the intensity by factors of 5-10, but will not shift the wavelength.

The PL wavelength can be shifted somewhat by changing the Si concentration or by changing the annealing time, both of which are expected to change the size of the Si nanocrystals. Figure 3 shows that the peak wavelength can be shifted from ~7600 Å to ~6900 Å by reducing the dose from $6 \times 10^{17}/cm^2$ to $3 \times 10^{16}/cm^2$ (at 400 keV energy). Reducing the dose reduces the nanocrystal size, and the results of Fig. 3 are in qualitative agreement with a quantum confinement picture in which the silicon bandgap increases as the particle size decreases [26] and thus quantum confinement has been invoked to explain some of the PL results in Si implanted SiO_2 [13-15].

The presence of Si nanocrystals in fused silica gives rise to strong optical absorption as shown in Fig. 4. The absorption edge shifts to higher energies as the dose (and therefore the particle size) decreases. Results in Fig. 4 are qualitatively consistent with quantum confinement also, but the shift in the absorption edge is much greater than the PL shift. In addition, the absorption edge and the peak PL occur at significantly different energies. Therefore, the PL radiation cannot be attributed to the usual band edge luminescence.

The absorption results can be analyzed to provide estimates of the absorption bandgap (E_g) associated with the Si nanoparticles. For amorphous semiconductors, the absorption coefficient α varies with photon energy (E) as [27]

$$(\alpha E)^{1/2} = B\,(E-E_g) \qquad (1)$$

Assuming that this model applies to Si nanocrystals in SiO_2, then a plot of $(\alpha E)^{1/2}$ versus E should give a straight line with an x-axis intercept of E_g. In Fig. 5, the absorption coefficient data for the sample implanted to $6 \times 10^{17}/cm^2$ is plotted and compared to equation 1. The fit to the straight line is very good in the energy range from 3 to 4.5 eV and the intercept gives a bandgap of ~2.5 eV. At low energies, the linear fit deviates from the data possibly due to poorly defined band tails. At high energies, the curves deviate because the adsorption is saturated.

Adsorption bandgaps have been estimated for each sample in Fig. 4, and the results are plotted in Fig. 6 as a function of dose. Shown also in Fig. 6 is the energy of the peak PL for the same samples. In all cases, the PL occurs at significantly lower energies than the adsorption bandgap. Also, the bandgap increases considerably as the dose (particle size) decreases whereas the shift in the PL peak energy is very small. These factors are not consistent with a simple quantum confinement picture, and this suggests that states at the Si/SiO_2 interface may play an important role in the PL from Si nanocrystals in SiO_2 as suggested also by others [7]. The interface state model was originally invoked to explain PL results from porous Si [28] and it has been utilized to explaining PL results from nanocrystalline Si formed in SiO_2 by plasma chemical vapor deposition [29]. In this model, optical absorption in the nanocrystals is dominated by the size dependent change in the bandgap (as our optical absorption measurements suggest), but the excitation energy is transferred nonradiatively to surface or interface states, and PL results from trapping and localization of photoexcited carriers in the boundary states of the nanocrystal. Energies of surface states are relatively independent of nanocrystal size, and the PL would be expected to be almost constant for particles of different size as our results seem to suggest.

4. Compound semiconductor nanocrystals formed in SiO_2 and Al_2O_3

High-dose sequential implantation of selected combinations of ions followed by thermal annealing can be used to synthesize a number of compound semiconductor nanocrystals in a variety of host matrices [12, 17-25]. With this approach, the individual constituents of the

compound are implanted at energies chosen to give an overlap of the profiles. If the constituents are insoluble in the matrix and if they have a strong chemical affinity for each other, then compound formation is a likely result during annealing or during implantation at elevated temperature. Figure 7 shows that GaAs can be formed in SiO_2 [22]. In the as-implanted state, the x-ray diffraction spectra is featureless except for the Si (002) peak which is due to multiple scattering from the underlying substrate. After annealing, strong diffraction peaks are observed from zincblende GaAs, in addition to a broad scattering feature which arises from amorphous SiO_2. This shows that GaAs crystallites were formed during the annealing process. Also, implantation to these doses at RT destroys the short range order of the SiO_2 matrix, but the order is restored by annealing. The size and size distribution for GaAs nanocrystals in SiO_2 depend strongly on the order in which the ions are implanted [25]. If Ga is implanted first, the GaAs nanocrystals are much larger (up to 300 Å diameter) than in the case where As is implanted first (less than 100 Å diameter) after annealing at 1000°C. This size difference is believed to be related to the precipitation of Ga to form large precipitates when it is implanted first. These large precipitates then trap the As which is subsequently implanted, resulting in relatively large GaAs nanocrystals.

Group II-VI compound semiconductor nanocrystals can also be produced in SiO_2 by implanting various combinations of Group II and Group VI ions, followed by annealing [12] as shown in Fig. 8. X-ray diffraction shows that the hexagonal structure of CdSe is formed by implantation of Se + Cd, and the hexagonal structure of CdS results from the implantation of Cd + S. For the case of Cd + 0.5 Se + 0.5 S, diffraction peaks are intermediate between those of CdSe and CdS indicating that the mixed chalcogenide $Cd_1\ Se_{0.5}\ S_{0.5}$ has been formed by the implantation of three ions. This is supported by Raman measurements on the same samples. Nanocrystal size is (typically) less than 100 Å diameter.

Nanocrystals and quantum dots can be produced also in Al_2O_3 by ion implantation [12, 16, 21, 22]. Figure 9 shows x-ray diffraction results for the case of CdSe in (0001) Al_2O_3.

The θ-2θ scan along the Al_2O_3 c-axis shows the expected diffraction from the matrix, but there are also a multitude of diffraction peaks which arise from CdSe. These nanocrystals can exist as either hexagonal or cubic structures. X-ray results show that the hexagonal structure is favored if implantation is carried out at elevated temperature such that the Al_2O_3 matrix is not turned amorphous during implantation. The cubic phase of CdSe is favored if the implant turns the matrix amorphous. In Fig. 9, most of the hexagonal CdSe nanocrystals are oriented with their (002) planes parallel to the (001) planes of Al_2O_3. The (002) oriented hexagonal CdSe nanocrystals also exhibit strong in-plane alignment as demonstrated by φ scans (not shown). Consequently, the hexagonal CdSe nanocrystals in α-Al_2O_3 are three dimensionally oriented with respect to the host lattice. From TEM results (not shown), the CdSe nanocrystals of Fig. 9 are facetted with dimensions up to several hundred angstroms, and they exhibit strong band edge PL that is blue shifted by ~0.1 eV relative to that from the standard presumably as a result of quantum confinement. If smaller CdSe nanocrystals are produced, then a larger blue shift can be expected.

5. Compound semiconductor nanocrystals formed in silicon

Sequential implantation can be used also to form compound semiconductor nanocrystals in crystalline Si [17-21, 23]. X-ray diffraction results for several Group III-V compound semiconductor nanocrystals formed by sequential implantation into Si are shown in Fig. 10. The θ-2θ scans along the [001] direction of Si show the expected intense Si (004) reflection. In addition, there are strong peaks which arise from zincblende GaAs, GaP, InAs, and InP showing that these compounds were formed as a result of implantation and that the nanocrystals are oriented with their (001) planes parallel to the Si (001) planes. In each case, φ scans through the nanocrystal {202} reflections show fourfold symmetry which demonstrates that these nanocrystals are oriented in plane with their cube axes parallel to those of Si. Consequently, these compound semiconductor nanocrystals are three dimensionally oriented with respect to the silicon lattice. In the case

of GaP, the (004) reflections of Si and GaP cannot be resolved, but the (002) reflection demonstrates the presence of GaP since that reflection from Si is forbidden, and multiple scattering has been eliminated.

Implantation into Si was carried out at 500°C to preserve the crystallinity of the matrix. Results for (a), (b), and (d) in Fig. 13 are shown following annealing. In the as-implanted state, diffraction from the compound semiconductor was observed also, but reduced in intensity. The result for (c) in Fig. 10 is shown in the as-implanted state. Weak diffraction lines arising from In are observed also in the case of InP and InAs showing that some of the In is in the form of In precipitates, as noted previously by others [18]. Any unreacted As or P should be substitutional in the lattice, and there are no peaks which could be attributed to unreacted Ga.

For GaAs in Si, the microstructure and nanocrystal size depend strongly on the order of implantation, as shown in Fig. 11. The GaAs nanocrystals are considerably larger (up to a few hundred nanometers) if Ga is implanted first. If As is implanted first, the nanocrystals are smaller and the micrograph shows numerous Moire′ fringes which arise as a result of lattice mismatch between overlapped GaAs and Si. The difference in nanocrystal size depending on the order of the implant is believed related to the precipitation of Ga to form large precipitates if Ga is implanted first, because Ga is relatively insoluble in silicon. Arsenic is highly soluble in silicon, and when it is implanted first it should remain more uniformly distributed and should combine with the subsequently implanted Ga to form a more uniform distribution of smaller GaAs precipitates.

The driving force for the formation of these compounds in silicon as well as in the other materials is their strong chemical affinity for each other [18-20, 23, 30]. For the case of GaAs in silicon [23], the free-energy change for the precipitation of GaAs from solution is estimated to be -0.53 eV/atom at 1000°C, which is a very strong driving force for compound formation. The free energy of the compound relative to that of other possible compounds or the free energy of mixing of Si solid solutions therefore provides a

convenient criteria to determine whether compound formation will take place, assuming there are no kinetic barriers.

For compound semiconductor nanocrystals in silicon, integrated x-ray diffraction rocking curves from the implanted samples can be compared with diffraction results from samples where a compound semiconductor film is deposited epitaxially by MBE to determine how much of the implanted material combines to form the desired compound. We have made such a comparison for Ga and P implanted into silicon compared with MBE deposited GaP (600 Å thick) on silicon. Our initial results show that more than 60% of implanted Ga is combined to form GaP following annealing at 800°C/1 h. This is a lower limit, but it shows that efficiency for formation is large, and the efficiency may approach unity with an extended time of annealing or higher temperatures.

6. Conclusions

A wide range of nanocrystals and quantum dots can be produced in host materials such as SiO_2, α-Al_2O_3, and crystalline silicon. Si nanocrystals formed by ion implantation into SiO_2 exhibit strong PL in the near infrared region and strong absorption in the visible and UV regions. A small blue shift in the PL peak intensity is measured when the dose (and hence the particle size) is reduced. The shift of the absorption edge with dose is much larger, and this suggests that Si/SiO_2 interface states may play an important role in the PL.

The synthesis of a wide range of compounds by sequential ion implantation provides new opportunities for research in ion beam synthesis. Table I shows the compound semiconductor nanocrystals we have produced by sequential implantation into SiO_2, α-Al_2O_3, and crystalline Si, and results obtained by others are reported in references [17-20]. In amorphous SiO_2 nanocrystals are randomly oriented, but in crystalline matrices the nanocrystals are three dimensionally oriented. The size and size distribution depend on the dose, the annealing conditions, and the order of the implant. Compound semiconductor nanocrystals incorporated in some of these insulating materials may have interesting nonlinear optical properties [31], and ion implantation may be the most convenient way to

form some of these because of their sensitivity to temperature or extreme oxidizing conditions.

Acknowledgment

Oak Ridge National Laboratory, managed by Lockheed Martin Energy Research Corp. for the U.S. Department of Energy under contract number DE-AC05-96OR22464. Research at Fisk University is supported by DOE (DE-FG05-94ER45521) and at Vanderbilt University by Army Research Office (DAAH04-93-G-0123).

References

[1] See for example A. P. Alivisatos, *Science* **271**, 933 (1996).

[2] G. W. Arnold, *J. Appl. Phys.* **46**, 4466 (1975).

[3] K. Fukuami, A. Chayahara, M. Satou, J. Hayakawa, M Hangyo, S. Nakashima, *Jap. J. Appl. Phys.* **30**, L742 (1991).

[4] R. H. Magruder, L. Yang, R. F. Haglund, C. W. White, C. Yang, R. Dorsinville, and R. R. Alfando, *Appl. Phys. Lett.* **62**, 1730 (1993).

[5] R. H. Magruder, R. F. Haglund, L. Yang, J. E. Wittig, and R. A. Zuhr, *J. Appl. Phys.* **76**, 708 (1994).

[6] H. Atwater, K. V. Shcheglov, S. S. Wong, K. J. Vahala, R. C. Flagan, M. L. Brongersma, and A. Polman, *Mat. Res. Soc. Symp. Proc.* **316**, 409 (1994).

[7] T. Shimizu-Iwayama, K. Fujita, S. Nakao, K. Saitoh, T. Fujita, and N. Itoh, *J. Appl. Phys.* **75**, 7779 (1994).

[8] J. G. Zhu, C. W. White, J. D. Budai, S. P. Withrow, and Y. Chen, *Mat. Res. Soc. Symp. Proc.* **358**, 175 (1995).

[9] J. G. Zhu, C. W. White, J. D. Budai, S. P. Withrow, and Y. Chen, *J. Appl. Phys.* **77**, 4386 (1995).

[10] K. S. Min, K. Y. Shcheglov, C. M. Yang, H. A. Atwater, M. L. Brongersma, and A. Polman, *Appl. Phys. Lett.* **68**, 2511 (1996).

[11] W. Skorupa, R. A. Yankov, I. E. Tyschenko, H. Frob, T. Bohme, and K. Leo, *Appl. Phys. Lett.* **68**, 2410 (1996).

[12] C. W. White, J. D. Budai, J. G. Zhu, S. P. Withrow, D. M. Hembree, D. O. Henderson, A. Ueda, Y. S. Tung, and R. Mu, *Mat. Res. Soc. Symp. Proc.* **396**, 377 (1996).

[13] K. S. Min, K. V. Shcheglov, C. M. Yang, H. A. Atwater, M. L. Brongersma, and A. Polman, *Appl. Phys. Lett.* (in press).

[14] P. Mutti, G. Ghislotti, S. Bertoni, L. Bonoldi, G. F. Cerofolini, L. Meda, E. Grilli, and M. Guzzi, *Appl. Phys. Lett.* **66**, 851 (1995).

[15] T. Komoda, J. P. Kelly, A. Nejim, K. P. Harewood, P. L. F. Hemment, and B. J. Sealy, *Mat. Res. Soc. Sym. Proc.* **358**, 163 (1995).

[16] C. W. White, J. D. Budai, S. P. Withrow, S. J. Pennycook, D. M. Hembree, Jr., D. S. Zhou, T. Yo-Dihn, and R. H. Magruder, *Mat. Res. Soc. Symp. Proc.* **316**, 487 (1994).

[17] P. Madakson, E. Ganin, and J. Karasinski, *J. Appl. Phys.* **67**, 4053 (1990).

[18] S. Yu. Shiryaev, A. Nylandsted Larsen, and M. Deicher, *J. Appl. Phys.* **72**, 410 (1992).

[19] S. Yu. Shiryaev and A. Nylandstead Larsen, *Nucl. Inst. and Meth in Phys. Res. B* **80/81**, 846 (1993).

[20] A. K. Rai, R. S. Bhattacharya, and S. C. Kung, *Materials Letters* **13**, 35 (1992).

[21] C. W. White, J. D. Budai, J. G. Zhu, S. P. Withrow, R. A. Zuhr, Y. Chen, D. M. Hembree, R. H. Magruder, and D. O. Henderson, *Mat. Res. Soc. Symp. Proc.* **358**, 169 (1995).

[22] C. W. White, J. D. Budai, J. G. Zhu, S. P. Withrow, R. A. Zuhr, D. M. Hembree, D. O. Henderson, A. Ueda, Y. S. Tung, R. Mu, and R. H. Magruder, *J. Appl. Phys.* **79**, 1876 (1996).

[23] C. W. White, J. D. Budai, J. G. Zhu, S. P. Withrow, and M. J. Aziz, *Appl. Phys. Lett.* **68**, 2389 (1996); Addendum, *Applied Physics Lettrs* (in press).

[24] R. H. Magruder, J. E. Wittig, and R. A. Zuhr, *J. Non Cryst. Solids* **163**, 162 (1993).

[25] J. G. Zhu, C. W. White, D. J. Wallis, J. D. Budai, S. P. Withrow, and D. O. Henderson, *Mat. Res. Soc. Symp. Proc.* **396,** 447 (1996),

[26] T. Takagahara and K. Takeda, *Phys. Rev. B* **46**, 15578 (1992); B. Delley and E. F. Steigmeier, *Phys. Rev. B* **47**, 1397 (1993).

[27] N. F. Mott and E. A. Davis, Electronic Process in Non-Crystalline Materials (Clarendon Press, Oxford, England 1979) chapter 6.

[28] F. Koch, V. Petrova-Koch, and T. Muschik, *J. Luminescence* **57**, 271 (1993).

[29] S. Veprek, T. Wirschem, M. Rückschlob, C. Ossadnik, J. Dian, S. Perna, and I. Gregora, *Mat. Res. Soc. Symp. Proc.* **405**, 141 (1996).

[30] H. Hosono, *Jpn. J. Appl. Phys.* **32**, 3892 (1993).

[31] R. K. Jain and R. C. Lind, *J. Opt. Soc. Am.* **73**, 647 (1983).

Table 1.
Nanocrystal compounds formed by sequential implantation. An x indicates that the compound was formed in the given matrix.

	Substrate		
Nanocrystal	SiO_2	Al_2O_3	Si
SiGe	x	x	
GaAs	x	x	x
InAs	x		x
GaP	x		x
InP	x		x
CdS	x	x	x
CdSe	x	x	
$CdSe_{0.5}S_{0.5}$	x		
GaN		x	

Fig. 1. Z contrast cross-section TEM micrograph showing Si nanocrystals in SiO_2. Excess Si concentrations of (a) $5 \times 10^{21}/cm^3$ and (b) $2 \times 10^{22}/cm^3$ in SiO_2 were subsequently annealed (1100°C/1 h/Ar + 4% H_2) to cause nanocrystal formation.

Fig. 2. PL arising from Si (400 keV, $6 \times 10^{17}/cm^2$, RT) implanted fused silica in the as-implanted state and after anealing (1100°C/1 h).

Fig. 3. PL spectra from fused silica samples implanted by different doses of Si (400 keV) and annealed at 1100°C/1 h.

Fig. 4. Optical transmission (relative to an unimplanted sample) for fused silica samples implanted by Si (400 keV) to different doses and annealed at 1100°C/1 h.

Fig. 5. Plot of $(\alpha E)^{1/2}$ versus E for Si (400 keV, $6 \times 10^{17}/cm^2$, RT) implanted fused silica following annealing (1100°C/1 h).

Fig. 6. Dependence of adsorption bandgap and peak PL energy on ion dose for Si (400 keV) implanted in SiO_2 after 1100°C/1 h annealing.

Fig. 7. X-ray diffraction showing GaAs nanocrystals in SiO_2. Equal doses ($1.5 \times 10^{17}/cm^2$) of Ga and As were implanted into an SiO_2 film on a Si substrate. Diffraction results are shown in the as-implanted state and after annealing.

Fig 8. X-ray diffraction following the implantation of equal doses ($1 \times 10^{17}/cm^2$) of Group II ions and Group VI ions at energies chosen to give an overlap of the profiles. Implanted samples were annealed at 1000°C/1 h.

Fig. 9. X-ray diffraction showing CdSe nanocrystals in α-Al_2O_3. Equal doses ($4.3 \times 10^{16}/m^2$) of Se (at 330 keV) and Cd (at 450 keV) were implanted at 600°C and then annealed at 1000°C/1 h. The position and expected intensity (from powder diffraction files) of hexagonal and cubic CdSe are shown also.

Fig. 10. X-ray diffraction results showing the presence of Group III-V compound semiconductors formed by sequential implantation into Si. Implants were done at 500°C. Doses and energies used were

(a) $1 \times 10^{17}/cm^2$ each of Ga (470 keV) and As (500 keV),

(b) $8 \times 10^{16}/cm^2$ each of P (70 keV) and Ga (160 kev),

(c) $1 \times 10^{17}/cm^2$ each of As (180 keV) and In (220 keV), and

(d) $1 \times 10^{17}/cm^2$ each of P (120 keV) and In (320 keV).

Subsequent annealing was carried out at 1000°C/1 h for (a) and (b) and 800°C/1 h for (d). Sample (c) is in the as-implanted state.

Fig. 11. Cross-section TEM micrographs showing GaAs nanocrystals formed in Si by sequential ion implantation. Samples were implanted by equal doses ($1 \times 10^{17}/cm^2$) of Ga (470 keV) and As (500 keV) and annealed at 1000°C/1 h. Ga was implanted first in (a) and As was implanted first in (b).

Figure 1 (#401)
C. W. White

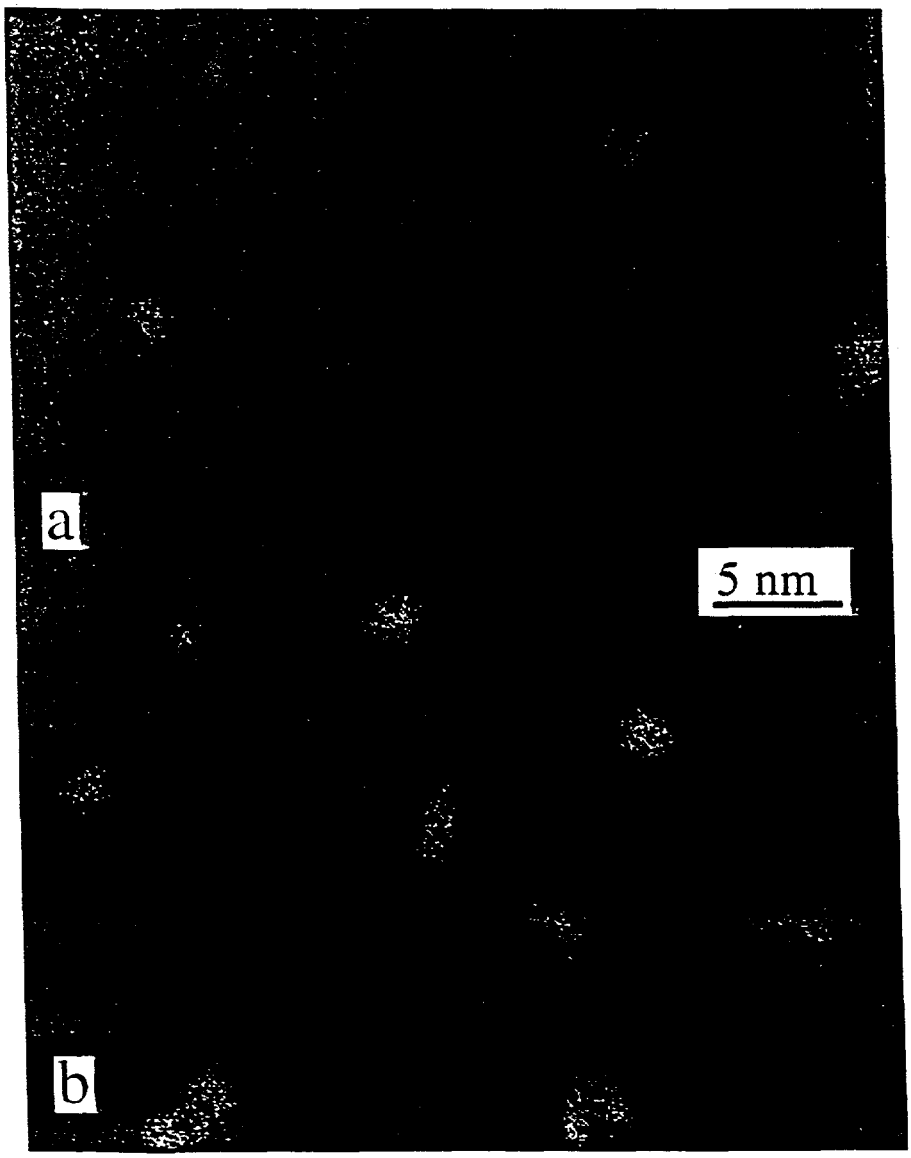

ORNL-DWG 94M-13438

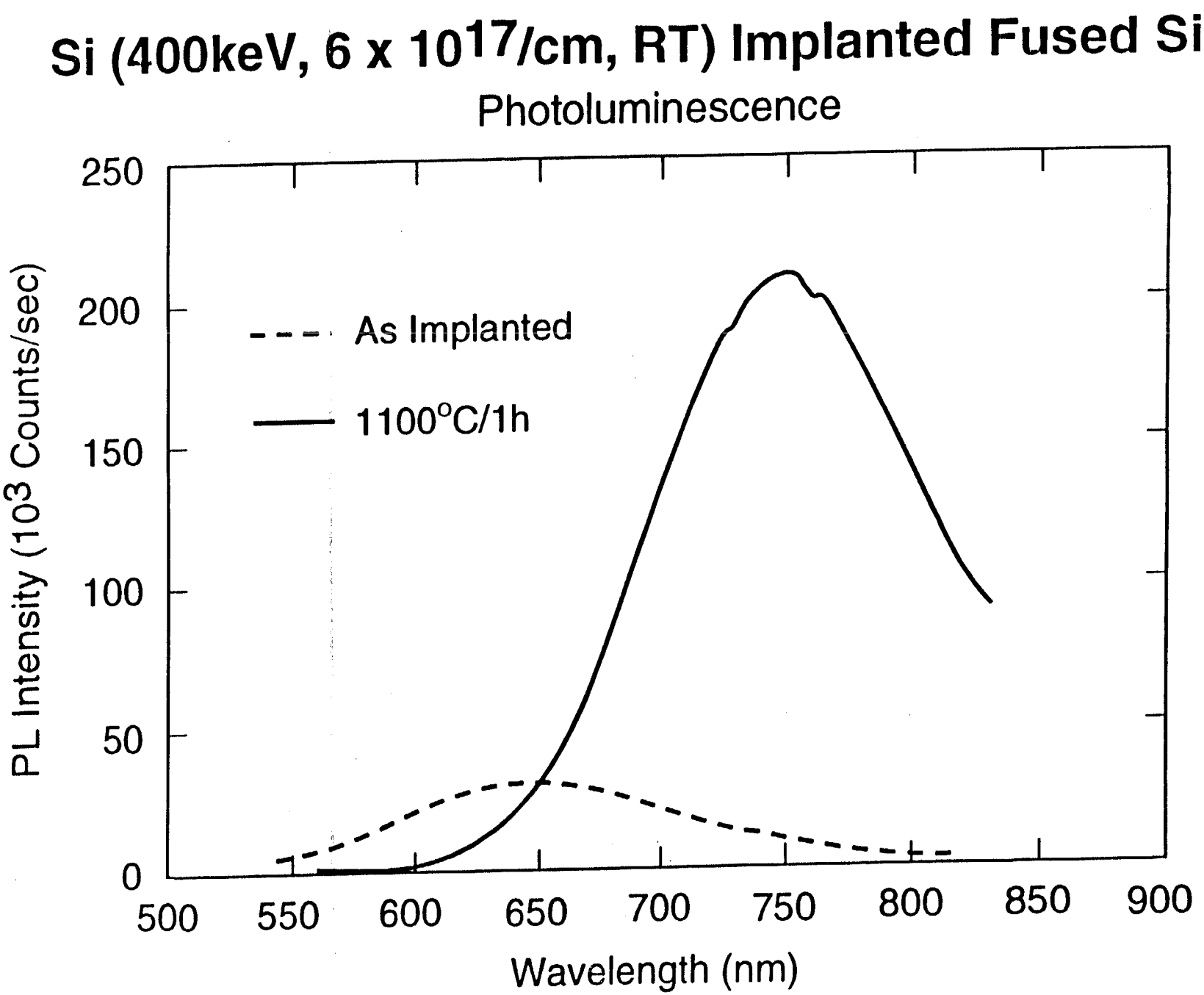

Figure 2 (#401)
C. W. White

ORNL-DWG 94M-13442

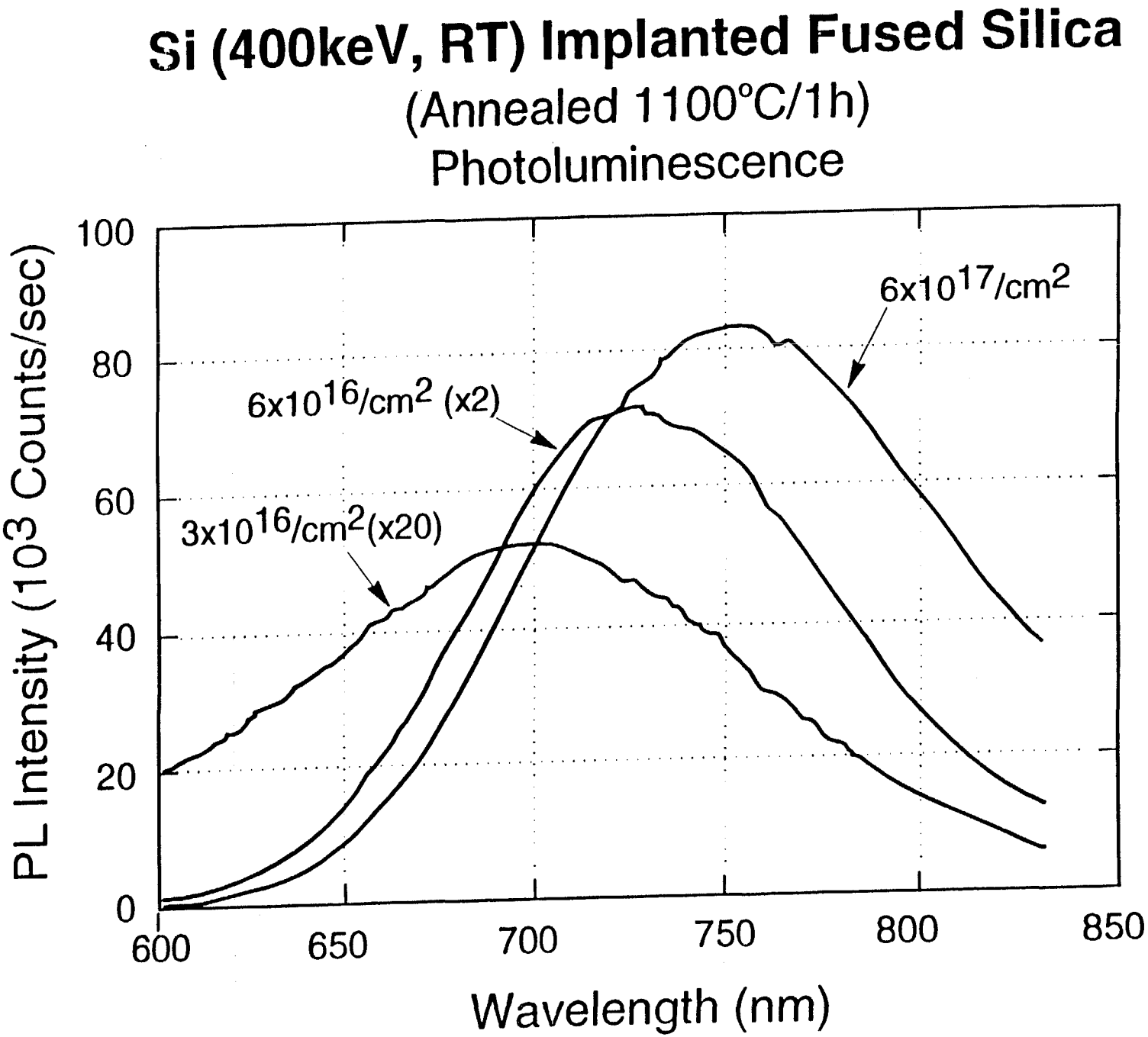

Figure 3 (#401)
C. W. White

Figure 4 (#401
C. W. White

ORNL-DWG 94M-13445

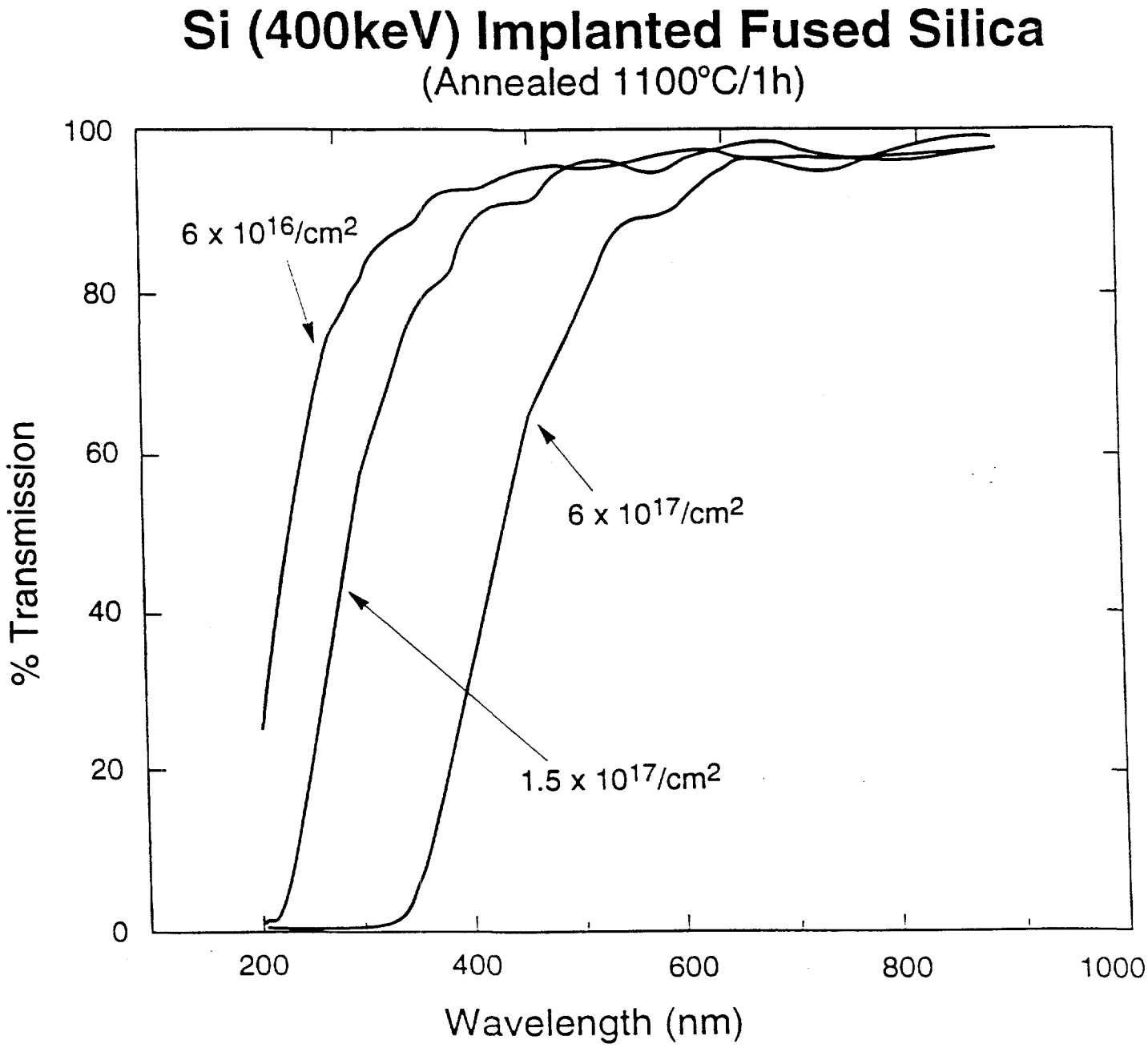

Figure 5 (#401)
C. W. White

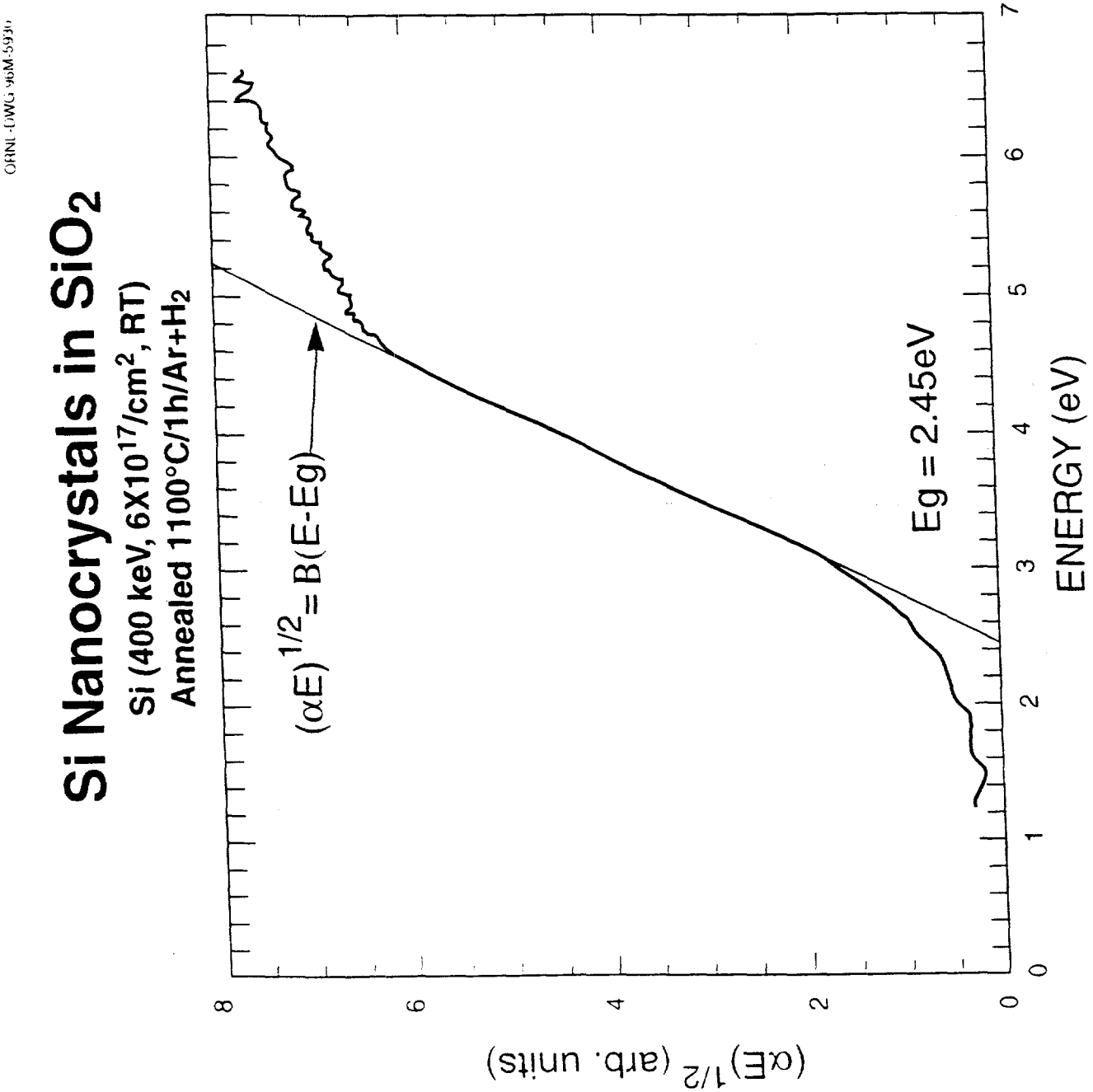

Figure 6 (#401)
C. W. White

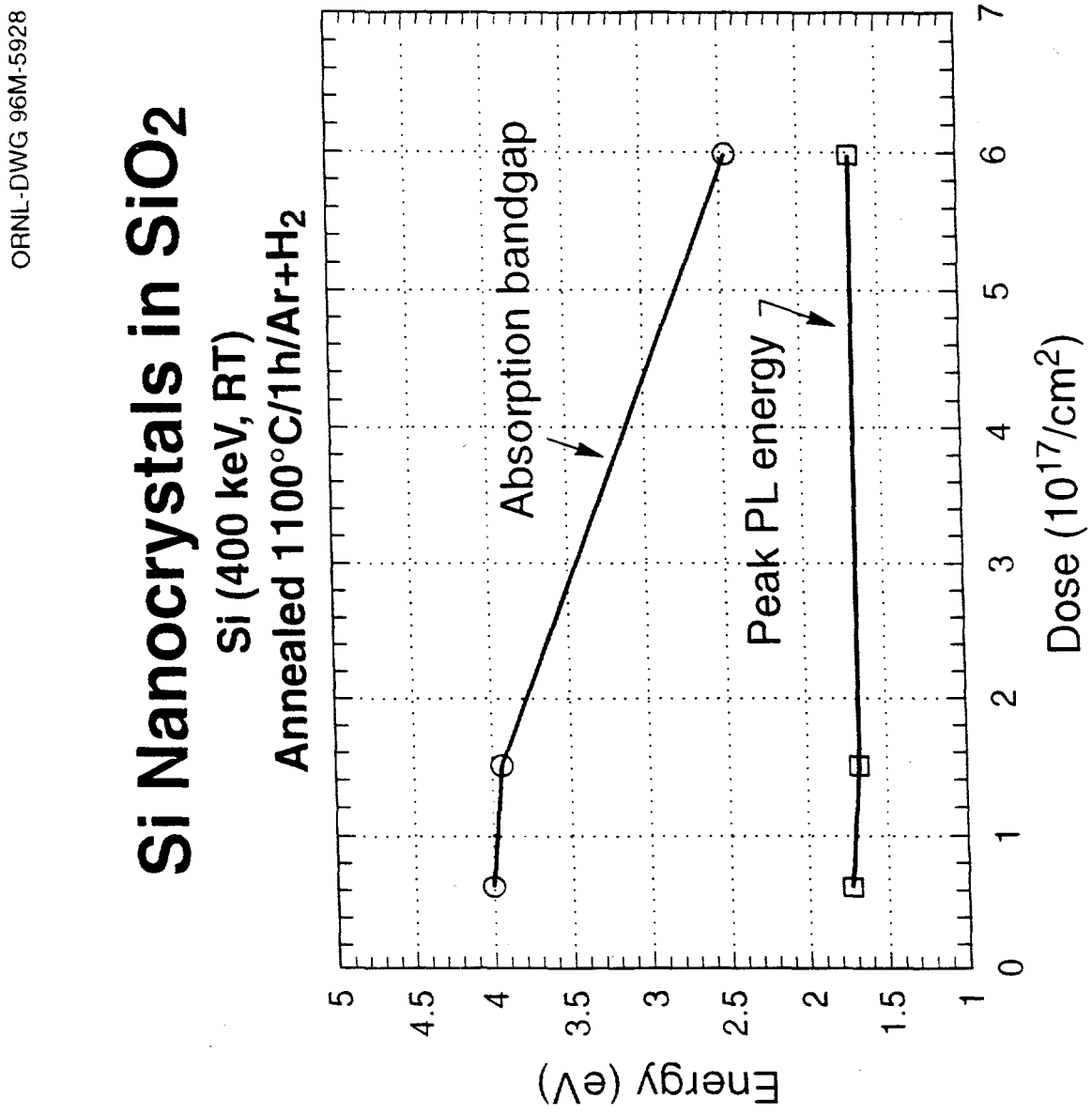

Figure 7 (#401)
C. W. White

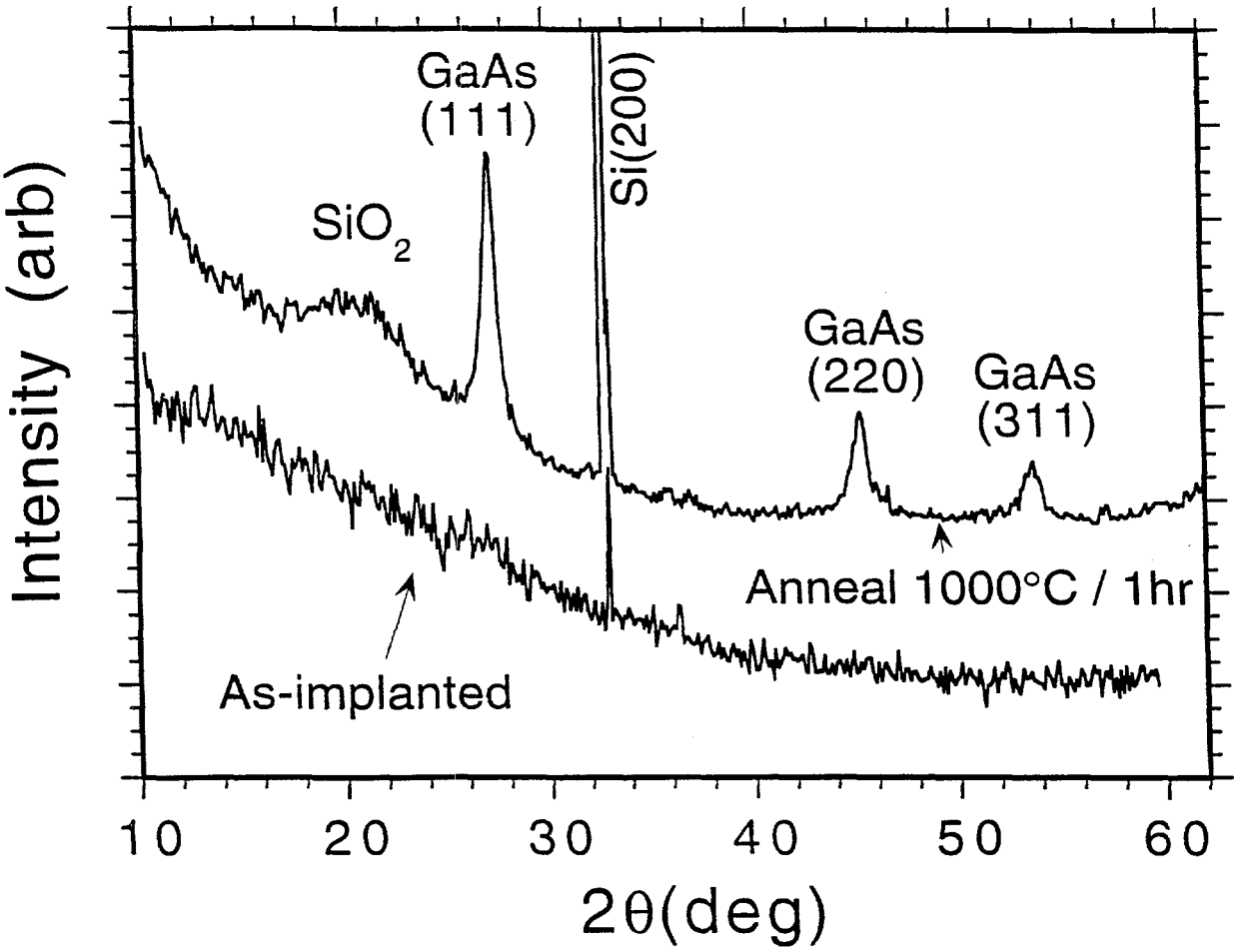

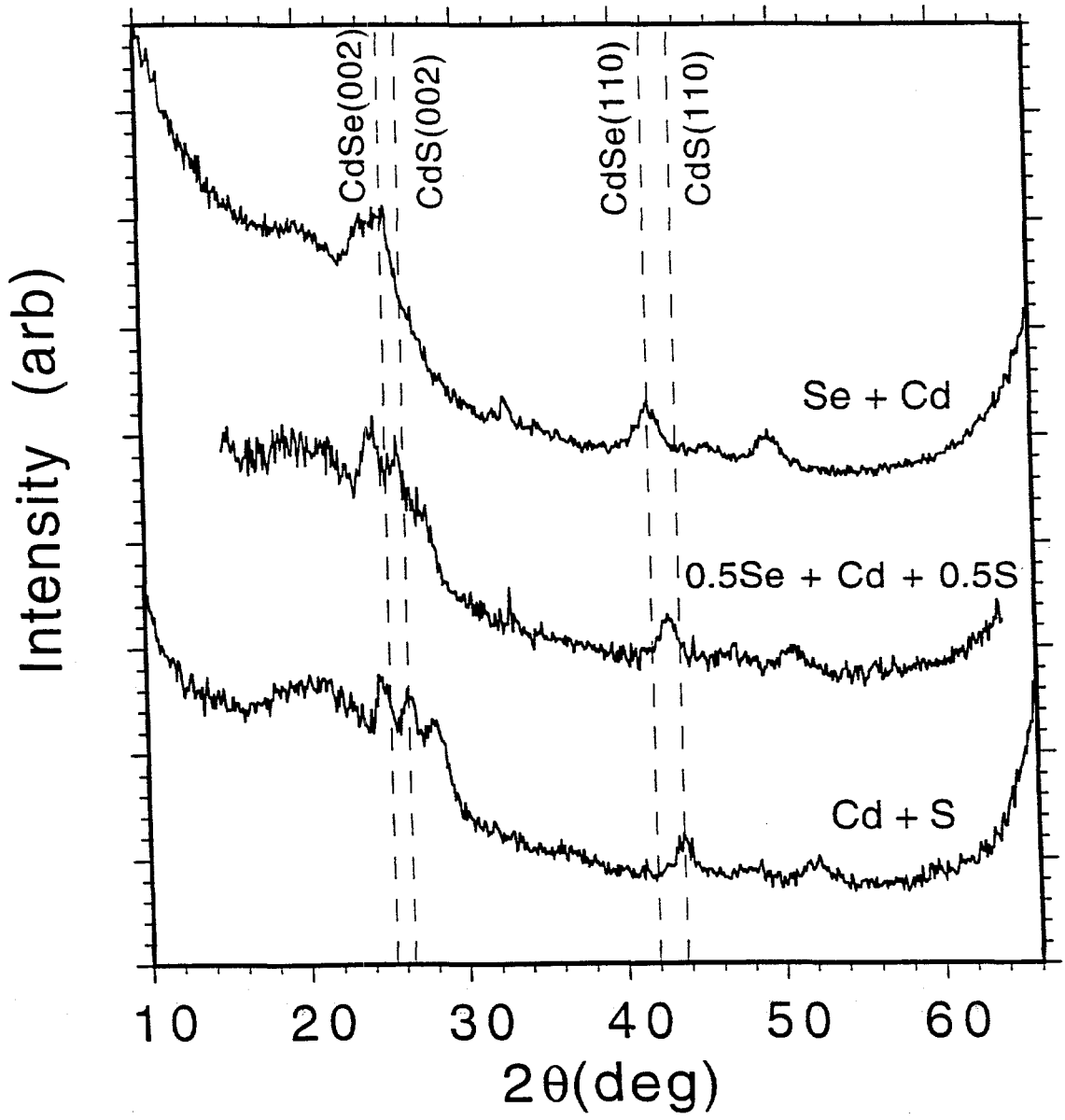
Intensity (arb)
CdSe(002)
CdS(002)
CdSe(110)
CdS(110)
Se + Cd
0.5Se + Cd + 0.5S
Cd + S
10
20
30
40
50
60
2θ(deg)

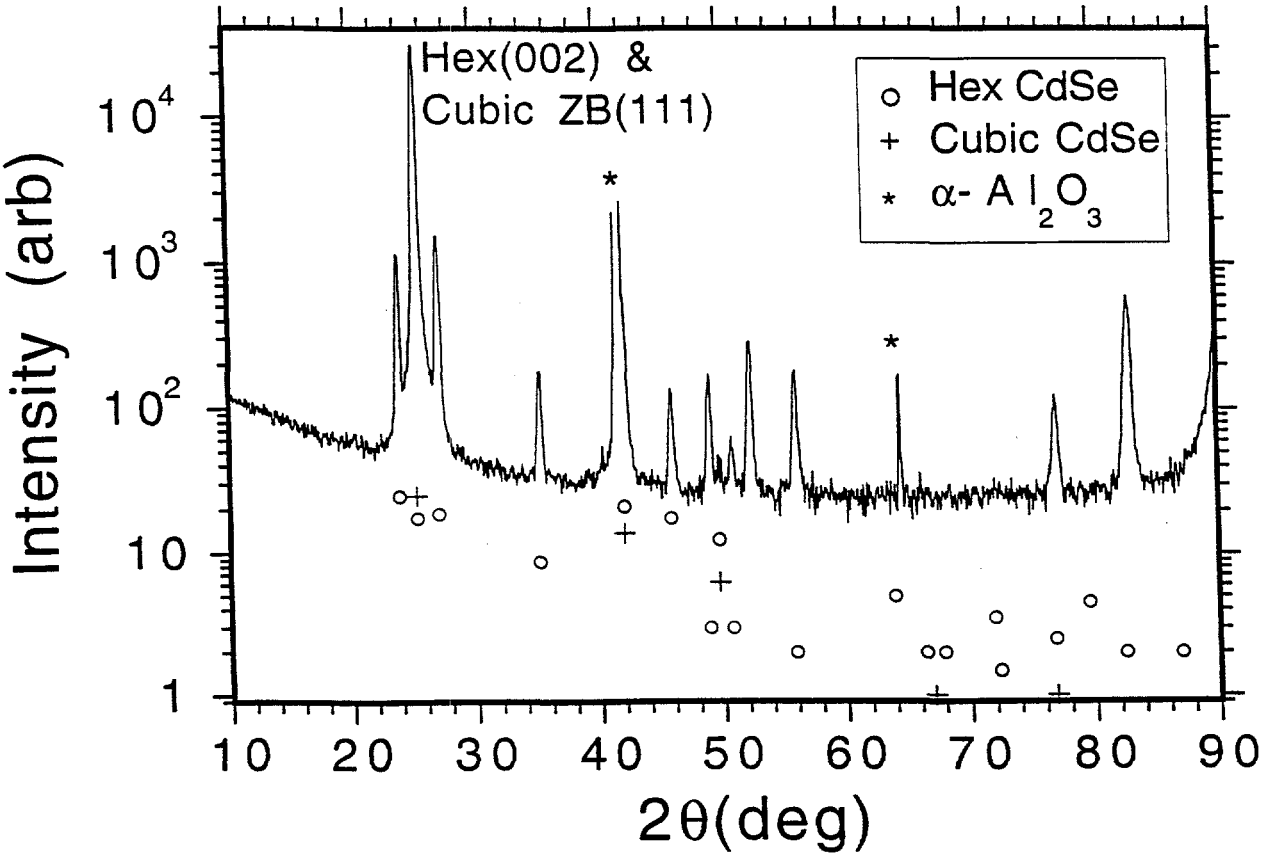
Hex(002) &
Cubic ZB(111)
Hex CdSe
Cubic CdSe
α- A l 2 O 3
Intensity (arb)
10^4
10^3
10^2
10
1
10 20 30 40 50 60 70 80 90
2θ(deg)

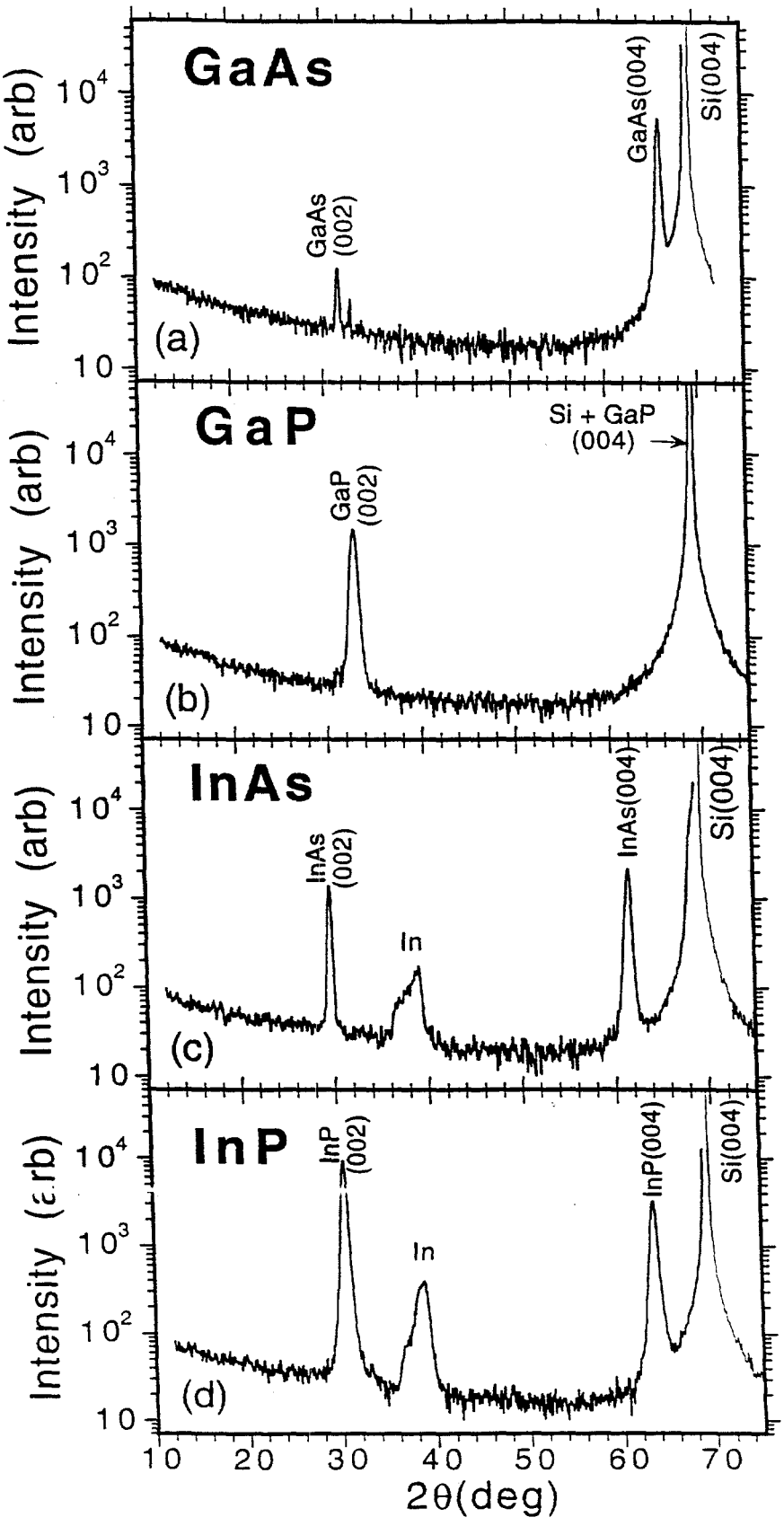
GaAs
GaAs(004)
Si(004)
GaAs (002)
(a)
Intensity (arb)
GaP
Si + GaP (004)
GaP (002)
(b)
InAs
InAs(004)
Si(004)
InAs (002)
In
(c)
InP
InP(004)
Si(004)
InP (002)
In
(d)
Intensity (arb)
10 20 30 40 50 60 70
2θ(deg)

Figure 11 (#401)
C. W. White

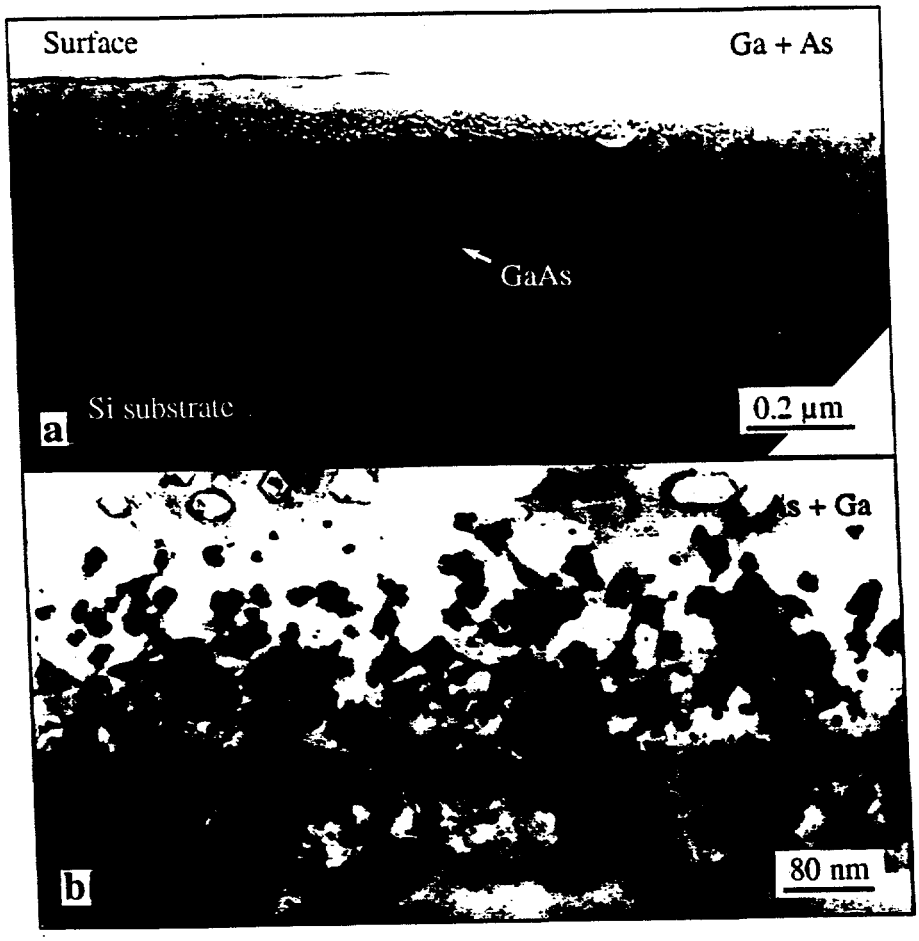

DISCLAIMER

This report was prepared as an account of work sponsored by an agency of the United States Government. Neither the United States Government nor any agency thereof, nor any of their employees, makes any warranty, express or implied, or assumes any legal liability or responsibility for the accuracy, completeness, or usefulness of any information, apparatus, product, or process disclosed, or represents that its use would not infringe privately owned rights. Reference herein to any specific commercial product, process, or service by trade name, trademark, manufacturer, or otherwise does not necessarily constitute or imply its endorsement, recommendation, or favoring by the United States Government or any agency thereof. The views and opinions of authors expressed herein do not necessarily state or reflect those of the United States Government or any agency thereof.